ISSN 1674-1056
http://cpb.iphy.ac.cn
http://iopscience.iop.org/cpb
中国物理 B
Chinese Physics
中国物理
Chinese Physics B

Single-order soft x-ray spectra with spectroscopic photon sieve

Yu-Lin Gao(高宇林), Lai Wei(魏来), Qiang-Qiang Zhang(张强强), Zu-Zua Yang(杨祖华), Wei-Min Zhou(周维民), Lei-Feng Cao(曹磊峰)
Citation: Chin. Phys. B . 2020, 29(5): 054101 . **doi:** 10.1088/1674-1056/ab81f0
Journal homepage: http://cpb.iphy.ac.cn; http://iopscience.iop.org/cpb

What follows is a list of articles you may be interested in

Dynamic shaping of vectorial optical fields based on two-dimensional blazed holographic grating

Xinyi Wang(王心怡), Yuan Gao(高源), Zhaozhong Chen(陈召忠), Jianping Ding(丁剑平), Hui-Tian Wang(王慧田)
Chin. Phys. B . 2020, 29(1): 014208 . **doi:** 10.1088/1674-1056/ab5a3b

Characterization of focusing performance of spiral zone plates with fractal structure

Hua-Ping Zang(臧华平), Cheng-Long Zheng(郑程龙), Zi-Wen Ji(吉子雯), Quan-Ping Fan(范全平), Lai Wei(魏来), Yong-Jie Li(李永杰), Kai-Jun Mu(牧凯军), Shu Chen(陈述), Chuan-Ke Wang(王传珂), Xiao-Li Zhu(朱效力), Chang-Qing Xie(谢常青), Lei-Feng Cao(曹磊峰), Er-Jun Liang(梁二军)
Chin. Phys. B . 2019, 28(6): 064201 . **doi:** 10.1088/1674-1056/28/6/064201

Internal and near-surface fields for a chiral sphere under arbitrary laser beam illumination

Bi-Da Su(苏必达), Ming-Jun Wang(王明军), Yue Peng(彭月), Su-Hui Yang(杨苏辉), Hua-Yong Zhang(张华永)
Chin. Phys. B . 2019, 28(6): 064210 . **doi:** 10.1088/1674-1056/28/6/064210

Numerical study of optical trapping properties of nanoparticle on metallic film with periodic structure

Cheng-Xian Ge(葛城显), Zhen-Sen Wu(吴振森), Jing Bai(白靖), Lei Gong(巩蕾)
Chin. Phys. B . 2019, 28(2): 024203 . **doi:** 10.1088/1674-1056/28/2/024203

Higher order harmonics suppression in extreme ultraviolet and soft x-ray

Yong Chen(陈勇), Lai Wei(魏来), Feng Qian(钱凤), Zuhua Yang(杨祖华), Shaoyi Wang(王少义), Yinzhong Wu(巫殷忠), Qiangqiang Zhang(张强强), Quanpin Fan(范全平), Leifeng Cao(曹磊峰)
Chin. Phys. B . 2018, 27(2): 024101 . **doi:** 10.1088/1674-1056/27/2/024101

Single-order soft x-ray spectra with spectroscopic photon sieve*

Yu-Lin Gao(高宇林)[1,2], Lai Wei(魏来)[3], Qiang-Qiang Zhang(张强强)[3], Zu-Zua Yang(杨祖华)[3], Wei-Min Zhou(周维民)[3], and Lei-Feng Cao(曹磊峰)[3,†]

[1] *Hi-tech Research and Development Centre, China Academy of Engineering Physics, Beijing* 100094, *China*
[2] *China Jiuyuan Hi-Tech Equipment Corporation Limited, Beijing* 100094, *China*
[3] *National Key Laboratory for Laser Fusion, Research Center of Laser Fusion, Mianyang* 621900, *China*

(Received 13 July 2019; revised manuscript received 26 December 2019; accepted manuscript online 23 March 2020)

A single-order diffraction transmission grating named spectroscopic photon sieve (SPS) for soft x-ray region is proposed and demonstrated in this paper. The SPS consists of many circular pinholes located randomly, and can realize both free-standing diffractions and the suppression of higher-order differations. In this paper, the basic concept, numerical simulations, and calibration results of a 1000-lines/mm SPS for soft x-ray synchrotron radiation are presented. As predicted by theoretical calculations, the calibration results of a 1000-lines/mm SPS verify that the higher-order diffractions can be significantly suppressed along the symmetry axis. With the current nanofabrication technique, the SPS can potentially have a higher line density, and can be widely used in synchrotron radiation, laser-induced plasma diagnostics, and astrophysics.

Keywords: higher-order diffraction suppression, extreme ultraviolet and soft x-rays, single-order diffraction grating

PACS: 41.85.Si, 42.25.Fx, 42.79.Dj **DOI:** 10.1088/1674-1056/ab81f0

1. Introduction

A conventional x-ray transmission grating (TG) consists of alternating transmissive and opaque nanometer structures, and is used in spectrometers to analyze the x-ray spectra radiated from high-energy-density processes, such as those in inertial confinement fusion and astrophysics.[1–6] According to the grating equation derived by Fraunhofer, it disperses x-rays not only in the first-order diffractions but also higher-order diffractions.[7] Unfortunately, the higher-order diffractions with various wavelengths may overlap each other in continuous or broadband spectra. Hence, a complex unfolding process must be performed to extract usable first-order diffractions,[2,5,6] which reduces the accuracy of the spectral data.

Sinusoidal transmission grating (STG) generates only one pair of conjugate first-order diffractions. Thus, they can be used to efficiently suppress higher-order diffractions in the optical region,[7] but they do not extend to x-ray region because of the inherent phase problem in material. In 2001, Kipp *et al.*[8] proposed a new zone plate, or photon sieve, with a large number of pinholes distributed appropriately over the Fresnel zones that focused soft x-rays to a sharp focal spot and suppressed higher orders. Other x-ray gratings that can suppress higher-order diffractions were developed, such as the binary sinusoidal transmission grating (BSTG),[9] the quantum-dot-array diffraction grating (QDADG),[10–12] and the quasi-sinusoidal single-order diffraction transmission grating (QSTG).[13] Unfortunately, the BSTG and the QDADG do not have line densities greater than 1000 lines/mm. Although a 1000-line/mm gold QSTG is fabricated, the x-ray-absorbing polymer membrane substrates must be used to support the periodic holes, which is also the case the BSTG and the QDADG encounter.

Here in this study, a two-dimensional (2D) diffraction grating that behaves as a spectroscopic photon sieve (SPS) is discussed. Because it has a large number of nanoscaled circular pinholes on a gold substrate, the SPS can be free-standing while suppressing higher-order diffraction components. An SPS with a spatial frequency of 1000 lines/mm is fabricated via electron-beam and x-ray lithography. The diffraction quality is calibrated with soft x-ray synchrotron radiation, and the results accord well with theoretical calculations. This grating offers new opportunities for improving the x-ray spectroscopy, monochromatization, and beam splitting.

2. Design of SPS

As shown in Fig. 1, the SPS consists of many nanoscale circular pinholes distributed on an opaque screen. The thin substrate (such as gold) was opaque to x-rays and was diced uniformly into $N \times N$ small squares with side length d, which was the period of this square dispersive device. In each square, a circular hole that transmits x-rays was randomly located within its area. Generally, the diameter (a) of the holes was half the value of d and was much larger than the wavelengths of the incident x-rays. Thus, the SPS was a 2D array of many

*Project supported by the National Natural Science Foundation for Young Scientists of China (Grant No. 11805179).
†Corresponding author. E-mail: leifeng.cao@caep.cn
© 2020 Chinese Physical Society and IOP Publishing Ltd

quasi-randomly distributed transmissive holes on a thin substrate that was opaque to x-rays.

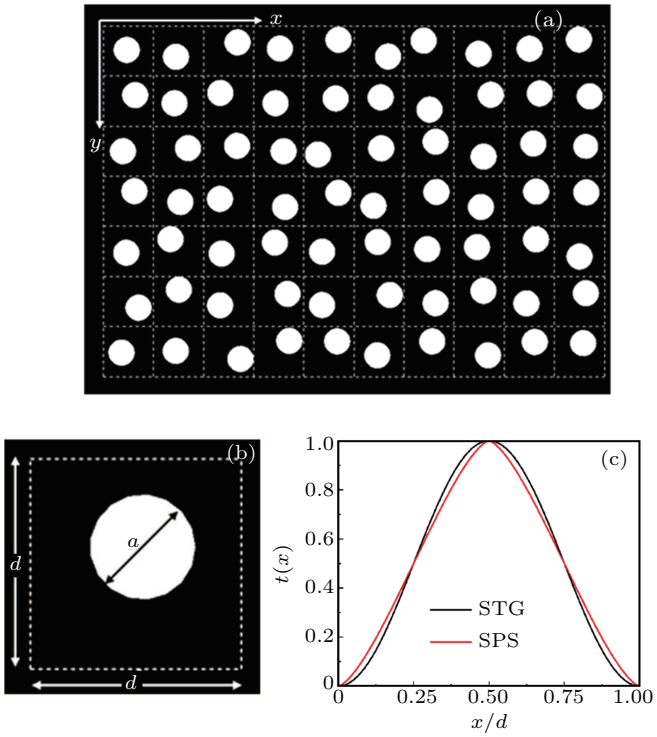


Fig. 1. SPS design, showing (a) design route, (b) one period of SPS, and (c) transmission function of SPS and STG within a period, with intensity being normalized with respect to $x = d/2$.

For a plane wave given by $A_0\exp(2\pi \mathrm{i}x/\lambda)$ incident on a TG with transmittance $\widetilde{t}(x)$ varying along the x axis, the classical Fourier optics theory predicts that the far-field diffraction pattern $\widetilde{U}(\xi,\eta)$ in the coordinate system shown in Fig. 2 can be written as

$$\widetilde{U}(\xi,\eta) = \frac{A_0\exp(\mathrm{i}kz)}{\mathrm{i}\lambda z}\exp\left(\frac{\mathrm{i}k(\xi^2+\eta^2)}{2z}\right) \times \int_{-\infty}^{+\infty}\int_{-\infty}^{+\infty}\widetilde{t}(x)\exp\left[-2\pi\mathrm{i}\left(\frac{x\xi}{\lambda z}+\frac{y\eta}{\lambda z}\right)\right]\mathrm{d}x\mathrm{d}y, \tag{1}$$

where $k = 2\pi/\lambda$ is the wave number of the incident light.

For the distribution along the ξ-axis, equation (1) is reduced to

$$\widetilde{U}(\xi,0) = \frac{A_0\exp(\mathrm{i}kz)}{\mathrm{i}\lambda z}\exp\left(\mathrm{i}k\frac{\xi^2}{2z}\right)\int_{-\infty}^{\infty} \times \int_{-\infty}^{\infty} t(x)\exp\left[-2\pi i\frac{\xi}{\lambda z}x\right]\mathrm{d}x\mathrm{d}y. \tag{2}$$

For an ideal STG with period d and silt width $d/2$, the amplitude of the transmission coefficient can be

$$t(x) = \frac{1}{2}+\frac{1}{2}\cos\left(\frac{2\pi x}{d}\right) = \frac{1}{2}+\frac{1}{4}\exp\left(\mathrm{i}\frac{2\pi}{d}x\right)+\frac{1}{4}\exp\left(-\mathrm{i}\frac{2\pi}{d}x\right). \tag{3}$$

From Eq. (3), only the zero-order diffractions and first-order diffractions exist, with no higher-order diffractions, after being modulated by an ideal STG.

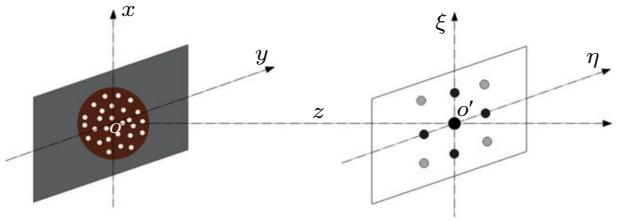


Fig. 2. Coordinate system for SPS geometry.

If the incident x-rays are transmitted only through the circular pinholes, the SPS transmittance is a real step function that is equal to one within the pinholes and zero on the substrate. In such a case, the variation of the SPS transmission function along the x axis can be written as

$$\widetilde{t_1}(x) = \lim_{N\to\infty}\frac{\sum_i 2\sqrt{(d/4)^2-(x-x_i)^2}}{Nd}, \tag{4}$$

where N is the number of pinholes along the x axis, and x_i is the transverse coordinate of the center of each hole located randomly within $[d/4, 3d/4]$ as shown in Fig. 1(b). The average number in a period of the holes can be written as the following expression

$$N = d/2\Delta x_i. \tag{5}$$

Substituting Eq. (5) into Eq. (4) yields

$$\widetilde{t_1}(x) = \lim_{\Delta x_i\to 0}\frac{\sum_i 4\sqrt{(d/4)^2-(x-x_i)^2}}{d^2}\Delta x_i = \frac{4}{d^2}\int\sqrt{(d/4)^2-(x-x_i)^2}\mathrm{d}x_i. \tag{6}$$

Then, the transmission function $\widetilde{t_1}(x)$ of the SPS within a period d can be depicted as

$$\widetilde{t_1}(x) = \begin{cases} \frac{1}{8}\left[\frac{\pi}{2}-\arcsin\left(1-\frac{4x}{d}\right)-\left(1-\frac{4x}{d}\right)\sqrt{1-\left(1-\frac{4x}{d}\right)^2}\right], & x\in[0,d/2], \\ \frac{1}{8}\left[\frac{\pi}{2}+\arcsin\left(3-\frac{4x}{d}\right)+\left(3-\frac{4x}{d}\right)\sqrt{1-\left(3-\frac{4x}{d}\right)^2}\right], & x\in[d/2,d]. \end{cases} \tag{7}$$

Figure 1(c) illustrates the amplitude transmission profile of the SPS within a period. It has a quasi-cosine transmission peculiarity similar to that of an STG. Thus, only zero-order and first order diffractions will exist after being modulated by an SPS, and higher-order diffractions will be eliminated.

Based on the above discussion, the SPS suggested here has approximately the same transmission function as that of an STG. When the number of circular pinholes N along the y axis is large enough, the SPS has the same amplitude transmission profile as the scenario along the x axis and will exhibit quasi-single-order diffraction as an ideal STG. Thus, the SPS will exhibit an approximate 2D single-order diffraction.

3. Simulation of the diffraction properties

To verify the SPS single-order diffraction property for soft x-rays, its far-field diffraction pattern was numerically simulated with Fresnel–Kirchhoff diffraction theory.[7] Parameters used in the simulation are given in Table 1.

Table 1. Parameters for diffraction pattern simulation of SPS.

Incident wavelength λ/nm	1
Incident angle/(°)	90
Period of SPS d/μm	1
Number of pinholes N	10000
Distance between the SPS and receiving screen Z/m	1.22
Pixel used in the receiving screen Δx/μm	5
Hits on the receiving screen $M \times N$	2048×2048
The thickness of the SPS h/μm	0.4

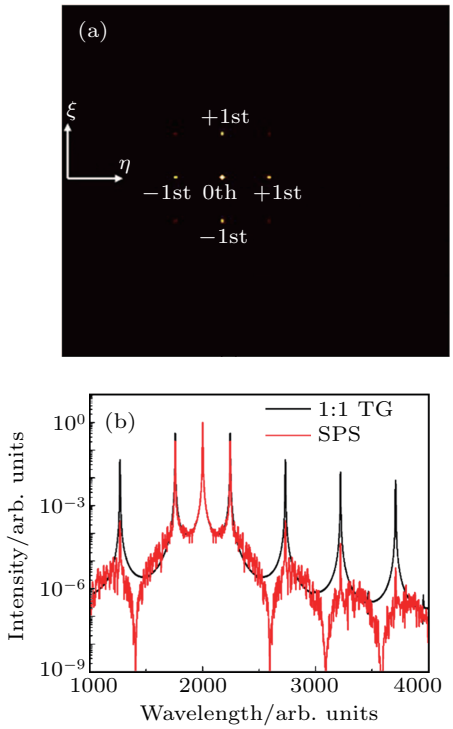


Fig. 3. (a) Calculated far-field SPS diffraction pattern at 1 nm, and (b) intensity profile of typical diffraction patterns of 1 : 1 TG and SPS at 1 nm.

The far-field diffraction pattern of the 1000-lines/mm SPS for an incident wavelength of 1 nm is shown in Fig. 3(a). The middle peak at the maximum intensity is the zero-order diffraction, and the others are all first-order diffractions. Along the η axis and the ξ axis, the SPS diffraction pattern has just a pair of first-order diffractions and one zero-order diffraction. In addition, according to the intensity profile in Fig. 3(b), even-order diffractions are eliminated and higher-order diffraction components are suppressed by about three orders of magnitude relative to that of the 1 : 1 TG. Although the relative diffraction efficiency (energy ratio of first-order to zero-order diffraction) of the SPS is only 21%, its application is acceptable for implementing the precise spectrum measurements and serving as a monochromatic source.

4. Calibration, experiments, and results

A hybrid of electron-beam and x-ray lithography were used to fabricate a high-line-density SPS for x-rays. First, the master mask for the SPS pattern was made by using the electron-beam direct-writing lithography. The task was implemented by the following steps: (i) SiC membrane with a thickness of 2 μm was used as substrate; (ii) a Cr (5 nm)/Au (10 nm) plating base was deposited on the substrate by using electron beam evaporation; (iii) after electron beam resist (ZEP520A) was spin-coated and baked, the SPS patterns were written in the electron beam resist by using the electron beam lithography system; (iv) the resist patterns were transferred into Au layer with a thickness of 300 nm by electroplating process. The second key step is the x-ray lithography, and the main steps are as follows: i) transfer the mask patterns into a positive ZEP520 A resist layer on a 0.2-μm-thick SiC membrane containing a Cr (5 nm)/Au (10 nm) plating base; ii) the x-ray lithography was carried out at beamline 3B1B1 of Beijing Synchrotron Radiation Facility with a resist thickness of 600 nm; iii) the resist patterns were transferred to the Au layer with a thickness of 550 nm by using the electroplating process and the resist mold was removed by using acetone followed by deionized water rinse; iv) the Cr/Au plating base and the SiC film beneath the resist mold were removed by ion beam etching and ICP etching, respectively.

Figure 4 shows the microstructure of a 1000-lines/mm SPS where the red lines indicate the periods. Because there were no isolated points on the opaque substrate, the SPScould be free-standing with no additional polymer membrane substrate for large areas. In addition, the apertures that transmit x-rays are circle. With 2-nm positioning accuracy[14] and 20-nm–40-nm resolution,[15] the technique could be used to fabricate an SPS with resolution reaching up to 5000 lines/mm.

The diffraction pattern of the fabricated SPS was characterized with a soft x-ray beam at the Beijing Synchrotron Radiation Facility. A cylinder mirror and flat-field grating were used as a monochromator to isolate single wavelengths

in a range of 50 eV–1500 eV. The energy resolution of the monochromator was $\Delta E/E = 10^{-2}$, and the divergence of the monochromatic x-ray beam was about 5.3 mrad in the axial direction. Figure 5(a) shows a schematic of the calibration arrangement. Various filters were used to eliminate high-order components in the quasi-monochromatic soft x-rays. An ultrafast mechanical shutter was used to control the luminous flux and to avoid trailing the source along columns of the detector. The x-ray detector was a back-illuminated charge-coupled device without an anti-reflection coating (Princeton Instruments, PIXIS-XO:1024B).

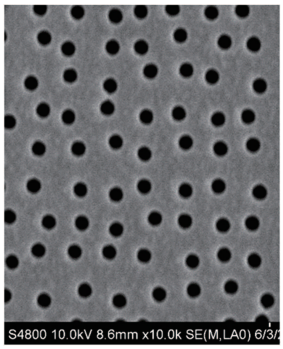


Fig. 4. Microstructure of fabricated SPS, with gold substrate thickness being 400 nm, the period 1000 nm, and the hole diameter nearly 500 nm.

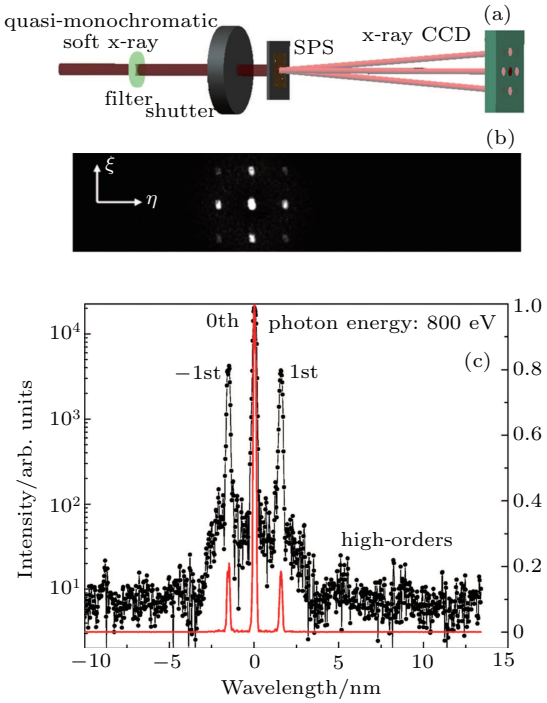


Fig. 5. Calibration of SPS. (a) Schematic diagram of experimental arrangement, with SPS being 100-μm wide and 200-μm high; (b) diffraction pattern recorded by CCD at 800 eV; (c) intensity profiles across η axis in Fig. 5(b), where red plot is in Cartesian coordinates, and black plot is log-scaled, and red plot is normalized to the peak intensity of zero-order diffraction.

Figure 5(b) shows the 2D SPS diffraction pattern imaged with an x-ray CCD at a photon energy value of 800 eV. Nine diffraction peaks appear, which are correlated with the calculated diffraction shown in Fig. 3(a). The rectangular diffraction spots arose from the rectangular shape of the SPS. Figure 5(c) shows the plots of one-dimensional intensity profiles across the η axis in Fig. 5(b). The red plot is in Cartesian coordinates, while the black plot has a log scale. As predicted by the theoretical calculation plotted in Fig. 3(b), only three diffraction peaks exist along the symmetry axis. Higher-order diffraction components have intensities that are only 0.47% of those for the first-order diffractions; they can be as low as the background radiation noise. The relative diffraction efficiency is 21.33%, which accords well with the theoretical value.

5. Conclusions

A new single-order diffraction transmission grating for the soft x-ray region is demonstrated. This spectroscopic photon sieve is comprised of many circular apertures, it is free-standing, and it can potentially have a higher linear density obtained by using the current nanofabrication technique. As predicted by theoretical calculations, the calibration results of a 1000-lines/mm SPS verify that higher-order diffractions can be significantly suppressed along the symmetry axis. It thus may become an alternative to conventional transmission gratings for high-accuracy x-ray spectroscopy.

Acknowledgments

The authors are grateful to Professor M Q Cui, Y D Zhao, and colleagues for their help in the calibration experiments, and also to Alan Burns, Ph. D, from the Liwen Bianji, Edanz Group China for editing the English text of a draft of this manuscript.

References

[1] Ceglio N M, Kauffman R L, Hawryluk A M and Medecki H 1983 *Appl. Opt.* **22** 318
[2] Eagleton R T and Tames S F 2004 *Rev. Sci. Instrum.* **75** 3969
[3] Eidmann K, Kishimoto T, Herrman P, Mizui J, Pakula R, Sige R and Witkowski R 1986 *Laser Part. Beams.* **4** 521
[4] Fill E, Stephan K H, Predehl P, Pretzler G, Eidmann K and Saemann A 1999 *Rev. Sci. Instrum.* **70** 2597
[5] Yang J M, Ding Y N, Zhang W H, Zhang J Y and Zheng Z J 2003 *Rev. Sci. Instrum.* **74** 4268
[6] Schriever G, Leben R, Naweed A, Mager S, Neff W, Kraft S, Scholze F and Ulm G 1997 *Rev. Sci. Instrum.* **68** 3301
[7] Born M and Wolf E 1970 *Principle of Optics*, 4th edn. (Oxford: Pergamon)
[8] Kipp L, Skibowski M, Johnson R L, Berndt R, Adelung R, Harm S and Seemann R 2001 *Nature* **414** 184
[9] Cao L F, Förster E, Fuhrmann A, Wang C K, Kuang L Y, Liu S Y and Ding Y K 2007 *Appl. Phys. Lett.* **90** 053501
[10] Wang C K, Kuang L Y, Wang Z B, Liu S Y, Ding Y K, Cao L F, Förster E, Wang D Q, Xie C Q and Ye T C 2007 *Rev. Sci. Instrum.* **78** 053503
[11] Wang C K, Kuang L Y, Wang Z B, Cao L F, Liu S Y, Ding Y K, Xie C Q, Ye T C and Hu G Y 2008 *Rev. Sci. Instrum.* **79** 123502
[12] Kuang L Y, Wang C K, Wang Z B, Cao L F, Zhu X L, Xie C Q, Liu S Y and Ding Y K 2010 *Rev. Sci. Instrum.* **81** 073508
[13] Kuang L Y, Cao L F, Zhu X L, Wu S C, Wang Z B, Wang Z B, Liu S Y, Jiang S E, Yang J M, Ding Y K, Xie C Q and Zheng J 2011 *Opt. Lett.* **36** 3954
[14] Spector S J, Jacobsen C J and Tennant D M 1997 *J. Vac. Sci. Technol. B* **15** 2872
[15] Anderson E H, Boegli V and Muray L P 1995 *J. Vac. Sci. Technol. B* **13** 2529